Author's Version

Hafnia-doped Silicon Bond Coats manufactured by PVD for SiC/SiC CMCs

by

Ronja Anton [a,*], Vito Leisner [a], Philipp Watermeyer [b], Michael Engstler [c], Uwe Schulz [a]

[a] German Aerospace Center (DLR), Institute of Materials Research, Cologne, 51147, Germany

[b] DLR, now at Max-Planck Institute für Eisenforschung GmbH, Düsseldorf, 40237, Germany

[c] Functional Materials, Department of Materials Science and Engineering, Saarland University, Saarbrücken, 66123, Germany

Acta Materialia (2020)

https://doi.org/10.1016/j.actamat.2019.10.050

Hafnia-doped Silicon Bond Coats manufactured by PVD for SiC/SiC CMCs

Ronja Anton [a,*], Vito Leisner [a], Philipp Watermeyer [b], Michael Engstler [c], Uwe Schulz [a]

[a] German Aerospace Center (DLR), Institute of Materials Research, Cologne, 51147, Germany

[b] DLR, now at Max-Planck Institute für Eisenforschung GmbH, Düsseldorf, 40237, Germany

[c] Functional Materials, Department of Materials Science and Engineering, Saarland University, Saarbrücken, 66123, Germany

*Corresponding author. E-mail address: ronja.anton@dlr.de (R. Anton).

Abstract

SiC/SiC ceramic matrix composites (CMCs) demand an environmental barrier coating (EBC) system when implemented in the hot section of a turbine engine. The connection between EBC and CMC is provided by a bond coat (BC). Numerous reasons make silicon the state-of-the-art BC material but it has some disadvantages regarding long time mechanical behaviour and oxidation resistance. To overcome this, a Si-BC doped with the refractory metal oxide HfO_2 is introduced. Two different compositions have been deposited on monolithic SiC by magnetron sputtering. After deposition the coatings are X-ray amorphous, homogenous, columnar structured and virtually free of cracks and pores. Furnace cycle tests up to 1000 cycles were performed at 1523 K. The evolution of microstructure and phases of the coatings were examined employing Scanning Electron Microscopy (SEM), Focused Ion Beam (FIB) serial sectioning, Transmission Electron Microscopy (TEM) and X-ray Diffraction (XRD). During high temperature exposure, the coatings crystallized and the silicon phase started to form a mixed thermally grown oxide (mTGO) layer. The BCs showed evenly distributed hafnia precipitates within the silicon. During testing Ostwald ripening of the precipitates took place. Hafnia slowly reacted with silicon oxide to hafnon ($HfSiO_4$). Compared to a pure silicon reference BC, the doped coatings show a better resistance towards crack initiation and spallation up to 1000 h testing time. The results demonstrate that sputtered hafnia-doped Si-BCs are more advantageous for SiC/SiC CMCs with respect to longevity, TGO adherence, and protection of the underlying SiC in comparison to pure Si bond coats.

Keywords: environmental barrier coating, ceramic matrix composites, physical vapour deposition, silicon, hafnia

1. Introduction

Since Ni-based-superalloys are reaching their operation temperature limit in the hot section of turbine engines, SiC/SiC CMCs seem to be the most promising candidates to replace that material. Several parts of SiC/SiC can already be found in commercial jet engines. Although SiC shows excellent oxidation resistance at high temperature, the material suffers deleterious loss in streaming water vapour [1–4]. Therefore, over the past 20 years a lot of development has been done concerning the protection of the substrate material by EBCs. The EBC system is supposed to protect the CMC against oxygen, streaming water vapour and to some extent against erosion [5–7]. EBCs usually comprise of several layers: starting with an oxidation protection base layer (usually pure Si), followed by the intermediate and the top layer, which need to protect the CMC from streaming water vapour [2,8]. While SiC evolves a slow growing oxide layer, it simultaneously builds up CO/CO_2. This gas formation may cause pore formation and

Acta Materialia; Anton et. al. 2020, https://doi.org/10.1016/j.actamat.2019.10.050

cracking of the material due to internal pressure. In addition, a composite SiC/SiC material cannot be manufactured completely dense, making the substrate vulnerable for internal oxidation. As the favourable material for the BC pure silicon has been used by various researchers and is widely accepted [9]. Its coefficient of thermal expansion (CTE) of $2.6 \cdot 10^{-6}$ K^{-1} is a close match to the CTE of SiC/SiC [10]. Adversely, its oxide SiO_2 can emerge in various polymorph phases - in most studies cristobalite is found. This polymorph undergoes a high/low temperature phase transitions with a CTE difference of about $7.2 \cdot 10^{-6}$ K^{-1} and a volume change of approximately 2.8 %. The transition causes tension between the SiO_2 layer and the non-oxidized Si coating. Therefore, it can lead to crack formation and terminate in spallation [11,12]. Moreover, the mechanical properties of silicon are strongly temperature dependent because of the brittle-ductile transition at about 898 K. Silicon has also a low fracture toughness of about 0.8-0.9 MPa $m^{1/2}$. Thereby, the low strength but high creep rates at high temperatures can cause delamination of the coating when the compressive stress gets too high [13,14]. Several concepts for improving the BC have been suggested but only little detailed information on the improvement of the BC is available. NASA developed HfO_2-Si based coatings potentially doped by rare earth metal or other dopants and manufactured mainly by Air Plasma Spaying and by electron beam directed vapour deposition (EB-DVD) for application temperatures above 1723 K [15–17].

The main goal of this paper is to improve both the chemical and mechanical properties and thus the longevity of the BC. This should be achieved by refractory metal oxide doping of the silicon BC and to assess the feasibility of manufacturing EBCs by PVD methods. Hafnium oxide seems to be well suited for this task because of its high melting point, high chemical stability in humid environment up to high temperatures, low vapour pressure and favourable phase stability. In combination with SiO_2, hafnia may be able to form hafnium silicate, i.e. Hafnon, as a reaction product. Hafnium silicate has a similar CTE to Si and low oxygen diffusivity. The increased molar volume of hafnium silicate compared to the initial silicon and hafnia could act favourably towards pore or crack closing [18]. Two variants of HfO_2-doped silicon coatings have been produced by magnetron sputtering which is a coating technology rarely used for EBC development so far. They have been tested under thermal cycling conditions at 1523 K. The microstructural evolution was analysed intensively employing both 2D and 3D image quantification techniques. Phase formation and oxidation behaviour in terms of long-time stability were analysed as well. For the first time, the mechanical properties of the doped coatings have been evaluated and compared to pure silicon coating. Finally, a preliminary assessment of the suitability of such BC variants for SiC/SiC CMCs is given.

2. Experimental

Monolithic α-SiC (Hexology SA, CoorsTek GmbH, Mönchengladbach, Germany) was used as model substrate material with a roughness of R_a = 0.3 µm, providing a relatively rough surface for PVD coatings and a chemistry similar to that of the CMC. The specimen dimension was 10 x 10 x 4 mm^3. The coatings were fabricated using a batch-type magnetron sputtering facility (Z 400, Systec SVS vacuum coatings, Karlstadt, Germany). Before coating deposition on one side of the specimen Ar^+-ion etching served as a cleaning process and to activate the specimen surface. Dense polycrystalline disks of Si and HfO_2 with a diameter of 100 mm were utilized as targets that were placed in a face-to-face arrangement. DC and DC/RF co-sputtering was performed at different target powers to achieve coatings with two different stoichiometries. To assure a stable coating process and to realize the different desired compositions, the power at the HfO_2 target was varied. The total pressure during deposition was 0.45 Pa in Ar atmosphere (flow rate at 25 sccm). During the process the substrate temperature reached about 400 K without

Acta Materialia; Anton et. al. 2020, https://doi.org/10.1016/j.actamat.2019.10.050

additional heating. The deposition rate was about 2 µm/h. The coated specimens underwent a furnace cycle test (FCT) in lab air. The hot time, here referred to as accumulated testing time, varied from 10 h until 1000 h. Each heating period of 60 minutes at 1523 K was followed by an active cooling period of 10 minutes in streaming air to nearly room temperature. One specimen of each kind has not been tested to examine the as-coated condition after deposition.

For all specimens phase analyses were performed using X-ray diffraction (XRD) (Siemens D5000, Cu-Kα radiation and secondary graphite monochromator, EVA/Topas 4.2 software package, Bruker AXS, Karlsruhe, Germany). High temperature XRD analysis (Bruker D8 Advance, Cu-Kα radiation, EVA/Topas 4.2 software package, Bruker AXS, Karlsruhe, Germany) was carried out to detect a possible cristobalite phase transition of the formed TGO. Therefore, a diffraction pattern was collected at room temperature, then at every 10 K starting from 453 K until 503 K and again after cooling to room temperature. The heating rate was 60 K/min. Microstructural analyses were carried out by scanning electron microscopy (SEM) (DSM Ultra 55, Carl Zeiss NTS, Wetzlar, Germany) equipped with an energy dispersive X-ray spectroscopy (EDS) system (Aztec, Oxford Instruments, Abingdon, UK). EDS analyses have been performed at 15 kV. To determine the distribution and development of the hafnia dopant phase, ImageJ has been used for digital image examination and quantification. Therefore, the particle size was determined by the feret diameter. Focused ion beam (Dual Beam FEI Helios, FEI Philips, Netherlands) serial sectioning technique was partly performed at Saarland University. This gave information about the three-dimensional connectivity and phase distribution which supported the two-dimensional analysis. The lamella specimen for the TEM analysis was produced by a focused ion beam (FIB) (Dual Beam FEI Helios, FEI Philips, Netherlands) preparation at DLR. An EDS mapping of the 500 h tested higher hafnia-doped BC via transmission electron microscopy (TEM) (Tecnai F30 TEM/STEM FEI Philips, Netherlands) was conducted to support the XRD findings. To understand the oxidation kinetics, weight curves have been recorded until 1000 h of FCT including one uncoated reference specimen of SiC. Since the coatings were applied on one side only, the weight change of the uncoated SiC was subtracted to extract the information of the coatings.

3. Results

3.1. Microstructure

3.1.1. As-coated

Since the open literature does not give any recommendations about the optimum composition of doped Si bond coats, the objective was to create a high doped and a low doped variant. The lower hafnia-doped BC had a content of dopant of 36 mol% the higher doped of 60 mol% HfO_2 molecules. Measuring the composition had been done by EDS of the as-coated BCs in cross section. A pure silicon BC was tested as a reference sample for comparison to the doped BCs. In Fig. 1 the as-coated variant of the silicon BC and the two doped BCs are shown in cross section and top view, respectively. No significant difference between the coatings was visible. All of them showed a columnar structure in the cross section as well as a cauliflower-like structure in the top view, both are typical features for coatings produced by magnetron sputtering. The layer thicknesses of the different variants were between 10 µm and 13 µm and originated from process parameter variations required to produce the BCs. The coatings appeared dense without pores or cracks and showed thorough adhesion to the substrate.

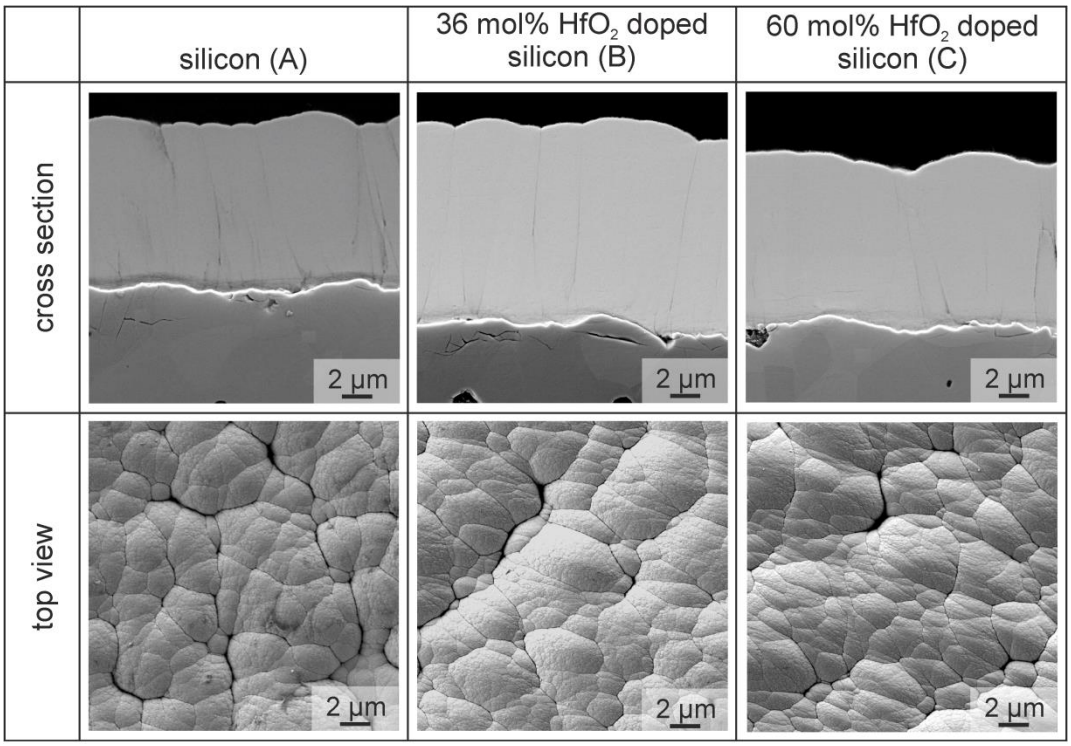

Fig. 1. BC in the as-coated state showing a columnar structure in cross section and cauliflower appearance of the columns in top view; A: silicon; B: 36 mol% HfO_2-doped silicon; C: 60 mol% HfO_2-doped silicon.

3.1.2. 10 h FCT

After 10 h of FCT the microstructures differed from the as-coated variants as seen in Fig. 2. On the surface of all BCs a thermally grown oxide (TGO) layer consisting of silica had formed. The pure silicon variant showed additional oxidation along the columnar gaps until the TGO on top had fully established. The doped BCs form hafnia-rich precipitates that were homogeneously distributed over the entire cross section. They were also located in the TGO layer making it a mixed thermally grown oxide (mTGO) layer consisting of silica and hafnia in the early stages of oxidation. Contrary to the pure silicon BC, the columnar gaps or column boundaries did not show any oxidation. The (mixed)TGO thickness appeared slightly larger in the higher doped variant than in the lower doped and pure silicon BC. The hafnia precipitates can be seen in the cross section. The entire surface appeared to be denser than the as-coated variant which applied to all the BCs after 10 h FCT due to the closed columnar gaps.

Acta Materialia; Anton et. al. 2020, https://doi.org/10.1016/j.actamat.2019.10.050

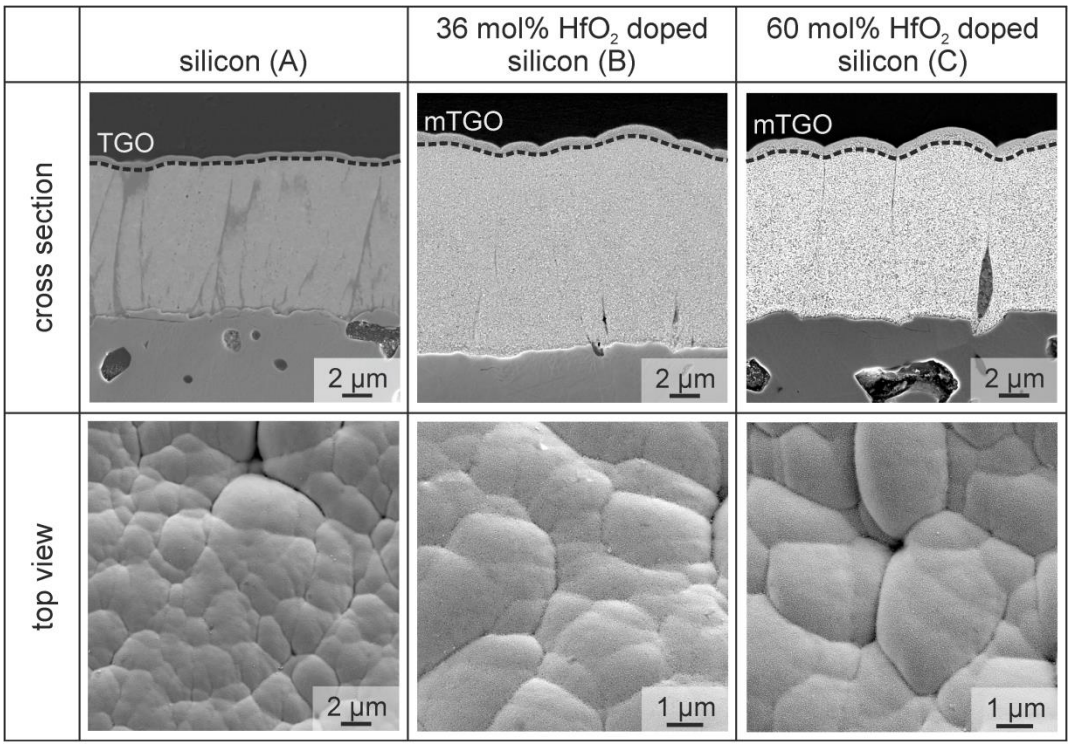

Fig. 2. BC and TGO/mTGO formed on top after 10 h of FCT testing at 1523 K; A: silicon; B: 36 mol% HfO_2-doped silicon; C: 60 mol% HfO_2-doped silicon.

3.1.3. 100 h FCT

The TGO grew with increasing testing time in thickness. The columnar structure almost disappeared for all coatings with longer testing time. While the columnar gaps of the Si-BC have been oxidized and filled, those gaps were no longer existent for both doped variants. After 100 h small cracks can be found within the TGO in Fig. 3 A cross section and top view of the Si-BC. The intercolumnar oxidation stopped while the TGO continues to grow. The lower hafnia-doped variant showed a mTGO with similar thickness as the pure BC without visible cracks. The hafnia precipitates were still homogenously distributed in both the initial BC and mTGO layer. The higher hafnia-doped variant, Fig. 3 C, showed a faster growing mTGO layer, but no crack formation can be associated with this growth. The spacing between the hafnia particles varied slightly within the mTGO but the overall distribution remained homogeneous.

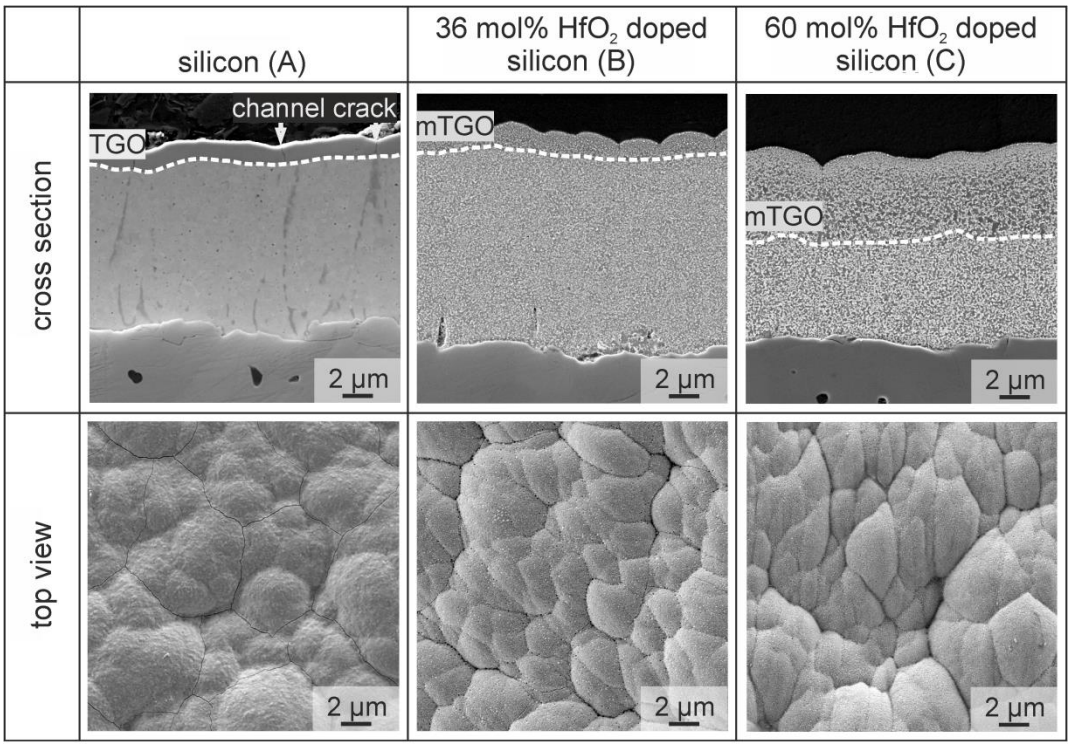

Fig. 3. BC and TGO/mTGO formed on top after 100 h of FCT testing at 1523 K; A: TGO develops channel cracking; B: homogenously distributed HfO_2 and thin mTGO layer; C: homogenously distributed HfO_2 and thick mTGO layer.

3.1.4. 1000 h FCT

Fig. 4 shows that all BCs visibly increased in thickness after 1000 h of testing. The Si-BC also experienced extensive oxide spallation due to crack formation. The cross section shows that approximately one third of the former coating consists of TGO. There, mud cracks expanded which were followed by coalescence and terminated in local spallation of the TGO. As a result, the non-oxidized part of the initial Si layer was exposed to the surface unprotected. From top view the initial silicon is clearly visible due to TGO spallation, see Fig. 4 A. The layer of both the lower HfO_2 content sample and the pure Si-BC consisted to approximately one third of (m)TGO and two thirds of initial coating. Agglomerated larger Hf-rich particles were locally detectable across large areas in the mTGO of the lower hafnia-doped variant whereas the lower part of non-oxidized silicon contained smaller hafnia particles. In some areas those large particles in the upper mTGO did not form and the hafnia has changed its size only slightly. Fig. 5 illustrates this variation in the mTGO microstructure for the 36 mol% HfO_2-doped BC after 1000 h FCT. SEM EDS analysis suggested that the large particles are hafnon ($HfSiO_4$). Within the higher doped variant, agglomerated hafnia-rich particles can be seen throughout the coating that were analysed as hafnon by XRD, see Fig. 4 C. They were still homogenously distributed in the BC. The entire BC was completely oxidized at the end of testing which means it consists only of mTGO without any residual silicon reservoir. This became clearly evident in the XRD analysis shown later in Fig. 10, too. Adhesion of both doped coatings was still good without any signs for spallation of the mTGO. Only widespread cracks were observed locally which seem not to harm the cohesion and adhesion of the BC, respectively. Although the doped BCs showed some cracks and the pure Si-BC even TGO spallation, the SiC substrate was unharmed and still protected by each BC variant since proper adhesion and cohesion of the coating was maintained. No enhanced oxidation was detected underneath vertical cracks.

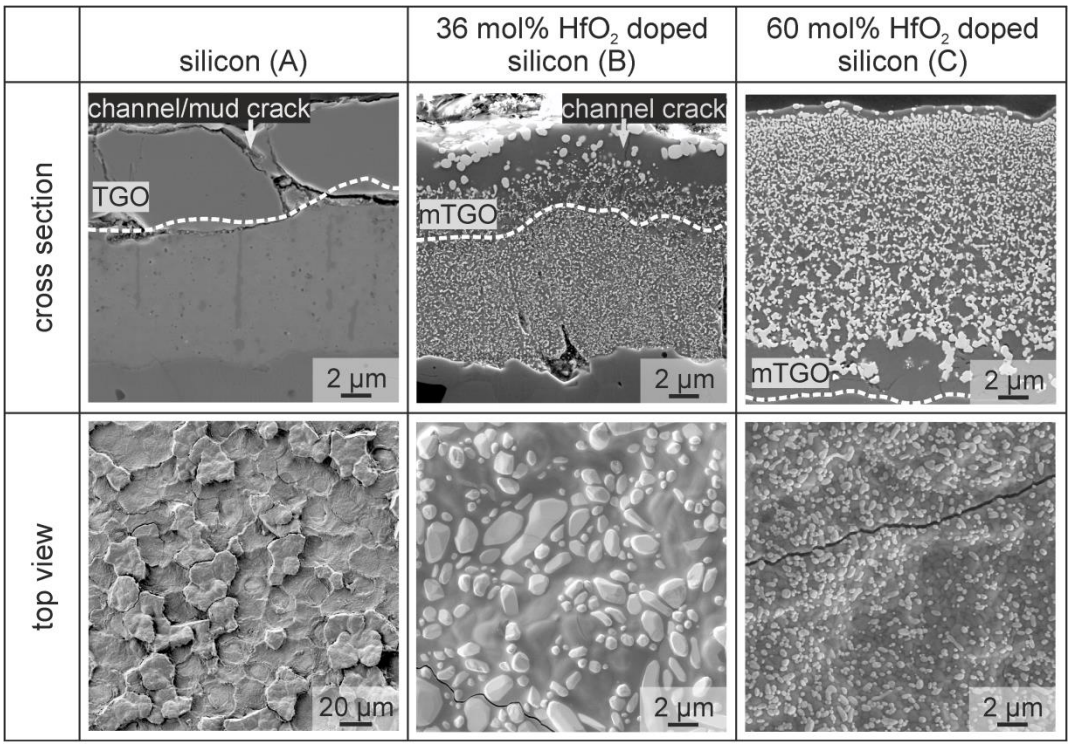

Fig. 4. BC and TGO/mTGO formed on top after 1000 h of FCT testing at 1523 K showing some crack formation after 1000 h of FCT testing at 1523 K; A: silicon showing partial TGO spallation and heavy cracking; B: 36 mol% HfO_2-doped silicon showing some channel cracks; C: 60 mol% HfO_2-doped silicon showing least vertical cracking.

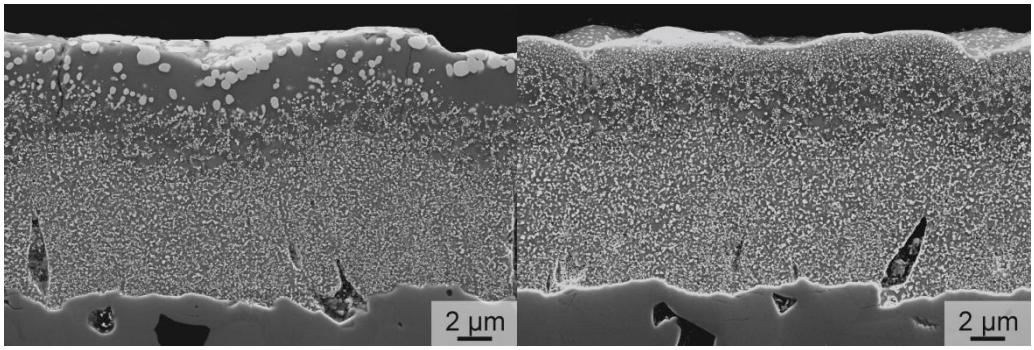

Fig. 5. Overview of the 36 mol% HfO_2-doped silicon BC after 1000 h of FCT testing at 1523 K showing variations in HfO_2 precipitate size and distribution along the coating.

3.1.5. Hafnia Particle Distribution

Based on the stacked Energy selective Backscattered (EsB) SEM pictures (Fig. 6 and Fig. 7) the increase in particle size and the decrease in particle number were clarified by histogram plots obtained via digital image examination. This allowed a detailed, quantitative analysis of the particles across the whole coating thickness. The lower hafnia-doped BC showed an increase in particle size and a decrease in overall particle number. Not completely visible in the SEM picture yet, the difference between 10 h and 100 h testing time became apparent in the histogram (Fig. 6). The trend towards fewer particles and simultaneously larger feret diameter can already be seen after 100 h of FCT but became more obvious after 1000 h FCT. The analysis has been done within an area of larger particles in the mTGO for the 1000 h FCT specimen as shown in Fig. 5 (left). To better visualize the changes in the smaller particle sizes with time, the histogram in Fig. 6 covers only 90 % of the particles and sizes above 300 nm are not

included. Therefore, the histogram excludes 13 particles at 10 h FCT, 19 particles at 100 h FCT, and 60 particles at 1000 h FCT. All particles were included for calculation of the mean.

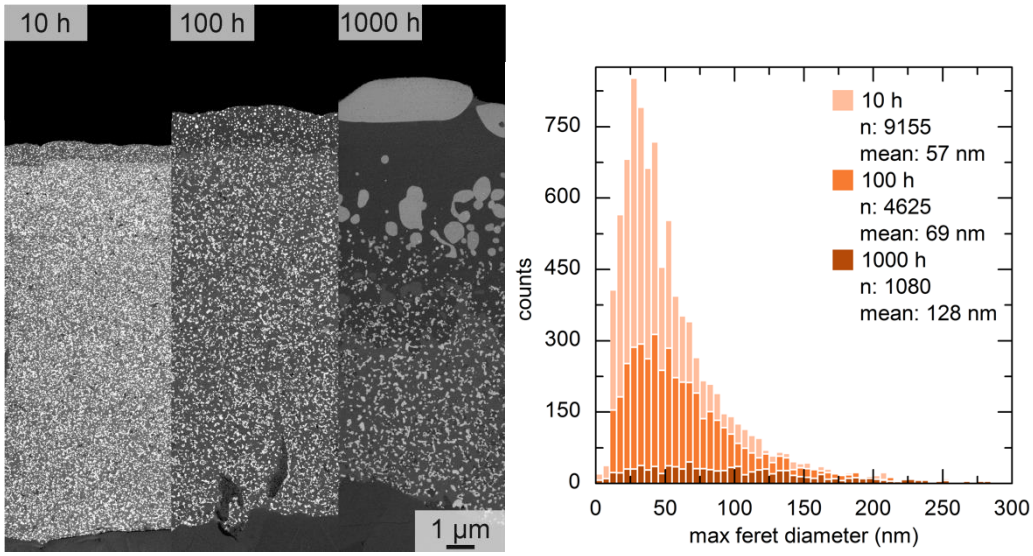

Fig. 6. Left: EsB-SEM cross section images of the 36 mol% HfO_2-doped Si-BC FCT for 10 h, 100 h and 1000 h; right: histogram of the max feret diameter distribution for the HfO_2/$HfSiO_4$ particles at the different testing times. The histogram shows only the first 90 % of the max feret diameter for a clearer visualization but all particles are considered in the statistics.

For the higher doped variant Fig. 7 also elucidates that the difference in the feret diameter between the analysed stages evolves more drastically between 100 h and 1000 h. The histograms largely overlapped between 10 h and 100 h. As in the lower doped BC, the 1000 h tested sample can be clearly separated from the others by its widely spread distribution of larger particles. In both 1000 h FCT variants hafnon and hafnia particles are combined to evaluate the distribution. Here, the histogram also shows only 90 % of the particles which excludes 42 particles at 10 h FCT, 7 particles at 100 h FCT, and 59 particles at 1000 h FCT.

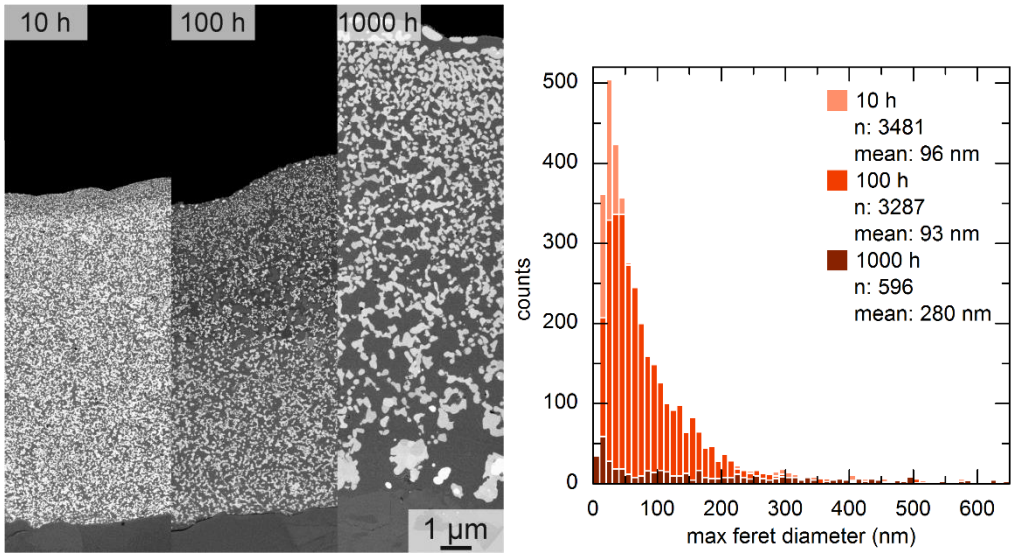

Fig. 7. Left: EsB-SEM cross section images of the 60 mol% HfO_2-doped Si-BC FCT for 10 h, 100 h and 1000 h; right: histogram of the max feret diameter distribution for the HfO_2/$HfSiO_4$ particles at the different testing times. The histogram shows only the first 90 % of the max feret diameter due to a clearer visualization but all particles are considered in the statistics.

Acta Materialia; Anton et. al. 2020, https://doi.org/10.1016/j.actamat.2019.10.050

The evolution in particle size throughout the coating was analysed in more detail in Fig. 8. Here, the stacked EsB-SEM pictures from Fig. 6 and Fig. 7 have been used to calculate the mean diameter of the particles represented by the feret diameter. Since the coatings were different in height the analysed area sizes differ. Therefore, the data has been equalized to the total thickness. Fig. 8 shows that although the distribution and shape is similar until 100 h FCT (see Fig. 6 and Fig. 7) the feret diameter varies with total dopant content. Up to 1000 h both variants developed larger particle sizes in different areas of the coating. With a lower content of hafnia the BC showed its largest particles near the surface only. In contrast, the higher doped BC had homogeneous particle sizes across the coating thickness. Only the 1000 h sample of the lower doped variant experienced an increase of about 400 nm in feret diameter.

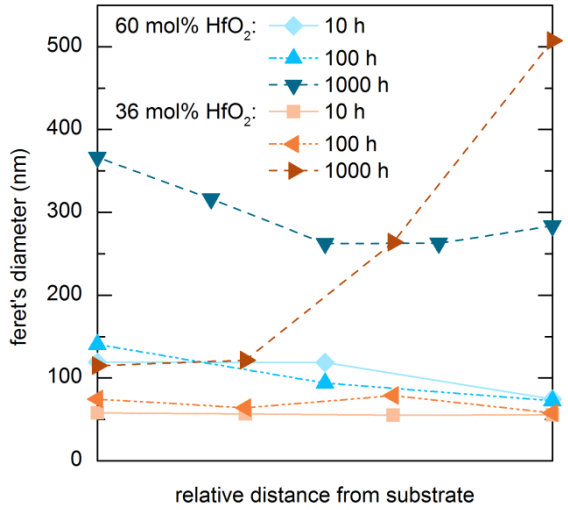

Fig. 8. Development of mean feret diameter in relative distance to the SiC substrate of the HfO_2/$HfSiO_4$ particles in the HfO_2-doped Si-BC FCT for 10 h, 100 h and 1000 h.

For better understanding of the morphology and microstructure, in particular the degree of connectivity of the dopant particles within the silicon, the FIB/SEM serial sectioning analysis supported the two-dimensional analyses. Only the 100 h tested hafnia-doped coatings have been analysed here. In both coatings two volumes from the transition zone from mTGO to the non-oxidized layer were selected. The lower doped BC showed that about 11.5 vol.-% of the particles was separated within the mTGO. Contrary, in the non-oxidized Si zone only 1.1 vol.-% of the particles did not belong to a hafnia network.

The provided data in Fig. 9 show clearly that the dopant in the high content variant formed a network of hafnia/hafnon particles throughout the BC. Hence, no difference can be seen between hafnia particles in the mTGO or hafnia particles in the Si region of the coating. Here, separated particles only count for about 0.1 vol.-% of the entire analysed volume.

Acta Materialia; Anton et. al. 2020, https://doi.org/10.1016/j.actamat.2019.10.050

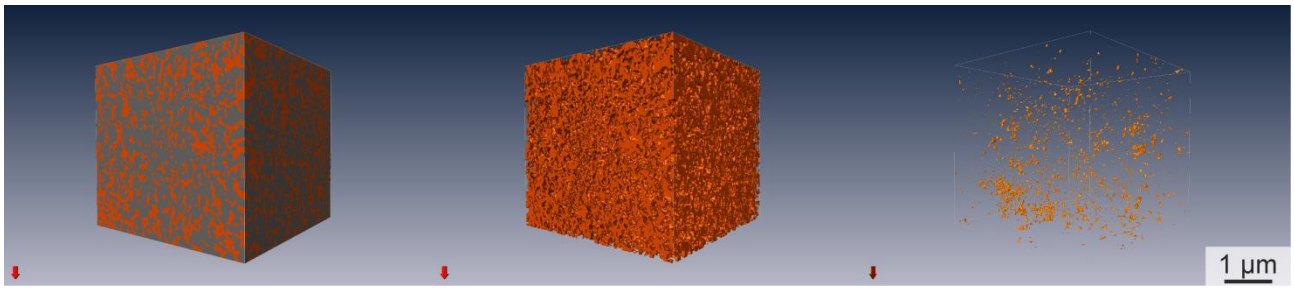

Fig. 9. 3D reconstruction of the 60 mol% HfO_2-doped Si-BC FCT for 100 h; HfO_2 particles in orange; Si/SiO_2/pores in grey; left: whole reconstruction; middle: only HfO_2 particles; right: free, unconnected HfO_2 particles.

3.2. Phase Analysis

All as-coated variants are X-ray amorphous. In this state, only peaks from the substrate material SiC can be detected. After the first heat treatment for 10 h the coatings were completely crystalized. In addition to the silicon phase, the silicon BC showed a growing cristobalite peak with cumulative testing time. Fig. 10 shows the phase evolution of the hafnia-doped BCs. After 10 h of testing silicon, hafnia and cristobalite were detected. The most significant transformation can be seen after 1000 h for the lower doped variant. There, the formation of hafnon from hafnia and silica is clearly apparent. Besides the hafnon phase, silicon oxide and hafnia were detected until 1000 h. The higher content BC showed the hafnon transformation already after 300 h FCT. With an increase of that phase with longer testing time, all hafnia particles were consecutively transformed into hafnon. The BC terminally comprises of only two phases: hafnon and cristobalite. The lower doped variant showed the first appearance of hafnon formation only after 1000 h testing time. There, silicon and hafnia are still detectable as well as cristobalite and hafnon.

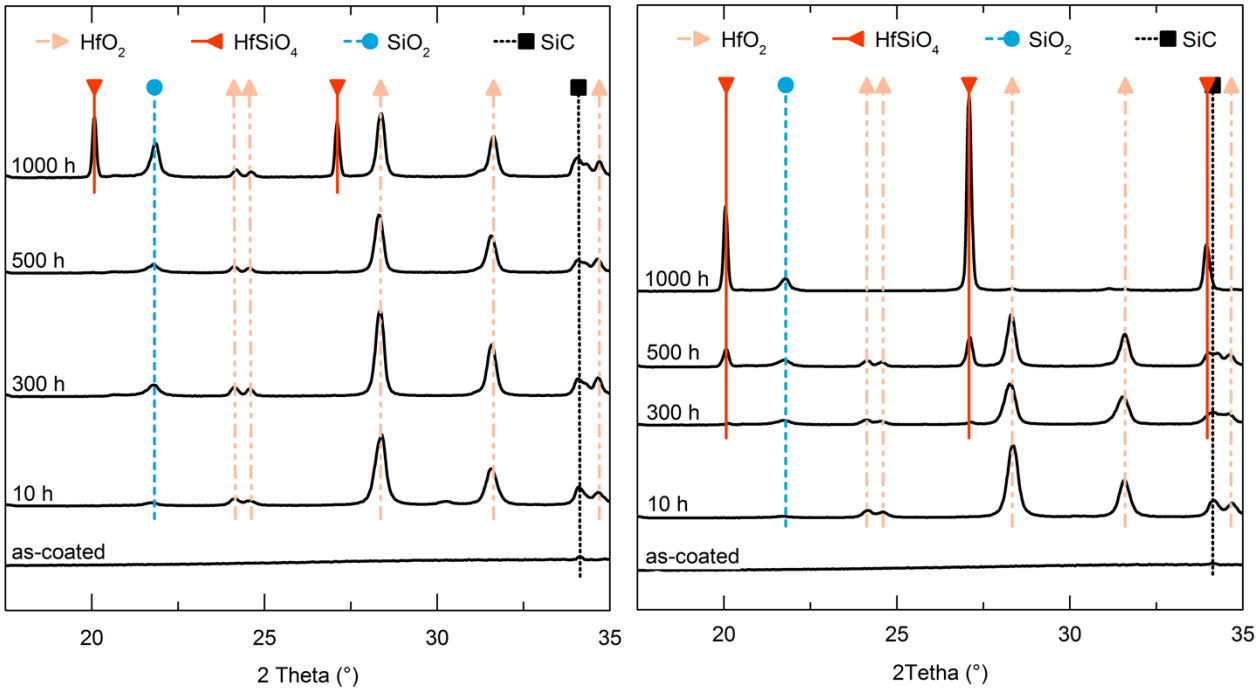

Fig. 10. Relevant part of the XRD scan from 15° - 35° 2θ of HfO_2-doped Si-BC for different testing times; left: 36 mol% HfO_2; right: 60 mol% HfO_2.

The EsB-SEM picture in Fig. 6 shows large hafnia-rich particles in the upper part of the coating. Their size allowed the confirmation of hafnon by SEM/EDS measurement in the mTGO. For smaller particles

an accurate measurement of their composition by EDS analysis in the SEM was not suitable. To further clarify and support the XRD and SEM/EDS findings, TEM analyses with EDS mapping were performed for selected sample conditions. Fig. 11 shows the lamella of the 500 h tested 60 mol% HfO_2-doped BC. The two red frames mark the areas where analyses have been conducted. The first one (area A) is closer to the substrate and the second one (area B) in the upper third of the coating closer to the surface, representing the transition zone between unoxidized reservoir and mTGO.

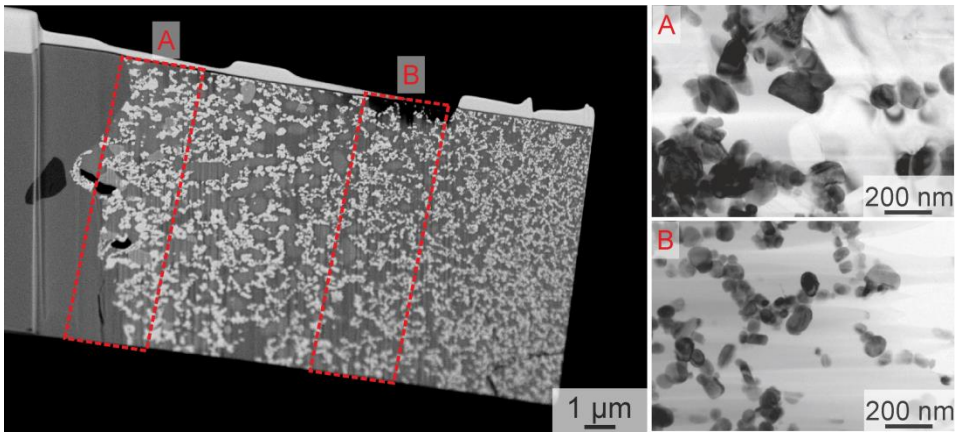

Fig. 11. Left: TEM lamella of the 500 h FCT 60 mol% HfO_2-doped BC with two red framed areas representing the regions of interest. Right: representative TEM bright-field images showing the hafnia precipitates of the 500 h tested 60 mol% HfO_2-doped Si-BC; A: close to the substrate; B: close to the surface.

Fig. 11 (right) shows two TEM bright-field pictures of the 500 h tested 60 mol% HfO_2-doped BC. The spherical round shape of the precipitates is clearly visible. They appeared to be adherent to each other instead of standing free in the silicon and silicon oxide matrix which supports the findings of the 2D and 3D analyses.

The single precipitates had a diameter of approximately 200 nm and smaller. Since they were not mono-crystalline, single crystal diffraction to identify the phases was impossible at this point. However, the EDS mapping helped to understand the phase transformation throughout the coating. Fig. 12 left shows area A of the BC close to the substrate. The mapping illustrates the separation between the hafnia precipitates and the silicon phase which clearly is not oxidized in this region.

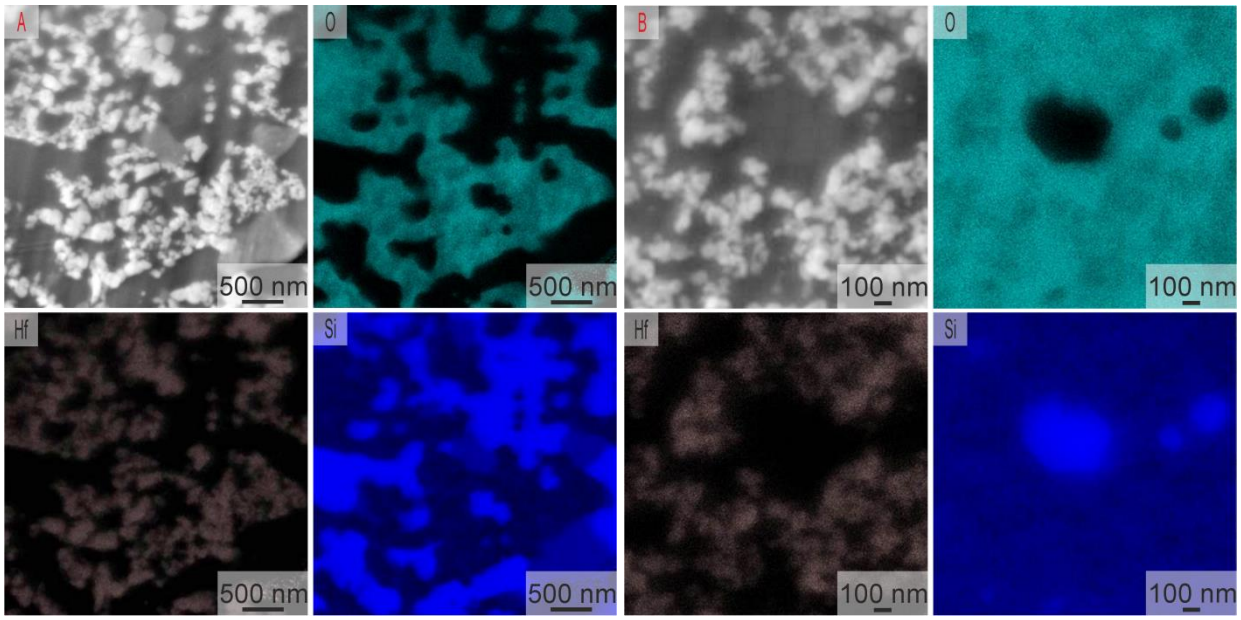

Fig. 12. TEM/EDS mapping of the 500 h tested 60 mol% HfO_2-doped BC; left: close to the substrate (A); right: close to the surface (B).

The second mapping shown in Fig. 12 is located in the upper third of the coating close to the surface (area B). Even though the section is within the considered mTGO, roundly shaped pure silicon phases can still be found. Since the silicon phases are the only larger parts with no hafnia, the mTGO seems to grow from the dopant particles into the silicon. Thereby, larger hafnia free areas need prolonged reaction time to form oxides. Except the residual silicon phases (bright Si-regions that are essentially oxygen-free in Fig. 12 B), both oxygen and silicon were distributed more evenly over the analysed area compared to Fig. 12 A. Therefore, a progressing phase transformation of hafnia into hafnon can be assumed but could not be unambiguously proven in the TEM analyses due to the very small particle sizes.

After detailed examination of the hafnia/hafnon phase, the growing SiO_2 phase was also analysed in more detail. As already mentioned, SiO_2 appeared as cristobalite in all BCs. Cristobalite is known for its transformation from high (beta) to low (alpha) temperature phase and vice versa. In order to investigate this transition, high temperature XRD was performed. The high and low temperature cristobalite phases can be distinguished by slightly different peak positions in the diffractogram. In the region of interest, alpha cristobalite (PDF 39-1425) has a peak at 21.9° 2θ while beta cristobalite (PDF 85-0621) has a peak at 21.4° 2θ. This shift starting from the low temperature phase transforming to the high temperature phase and back has been demonstrated in every BC variation shown in this paper. By employing high temperature XRD it was possible to determine the transition temperature to be at around 483 K. This phase transformation was the same for the doped and undoped coatings, despite remarkable difference in the phase assemblage of the three coatings (pure silica, mixture of silica + hafnia + hafnon for the low doped variant, and mixture of silica + hafnon for the high doped BC).

3.3. Oxidation kinetics

During FCT the oxidation kinetics and the underlying mechanisms can be analysed. The parabolic growth constant was determined by measuring the mass change per area as shown in Fig. 13. The TGO spallation of the Si-BC in Fig. 4 is not visible in the slope. Table 1 illustrates the mass change of the coatings after testing for 1000 h FCT. In order to determine the mass change of uncoated SiC a reference sample has

been tested as well. This leads to the different constants over different periods. Since the shape of the 60 mol% HfO_2-doped BC slope did not correspond to a straight line, the growth constant was calculated from 40 to 800 h FCT. Even though the slopes and the k_p values of the three materials SiC, Si and low hafnia differ from each other the underlying oxidation mechanism is supposedly the same. For the high hafnia variant a different mechanism can be assumed. Here, the hafnia network provides fast diffusion paths due to a large volume of connected hafnia particles. The slopes and the k_p values distinctly show that the BC with a lower dopant content has a slower growing mTGO. The growth rate of 36 mol% hafnia-doped BC is almost the same than that of the pure Si-BC.

Table 1 Mass change after 1000 h of FCT and parabolic growth constant of the BC variants over the testing time.

Bond coat	Mass change after 1000 h of FCT ($\mu g/mm^2$)	Growth constant (10^{-11} $kg^2/(m^4s)$)
SiC without BC	2.64	0.18 (0 – 1000 h FCT)
Si	8.99	2.21 (0 – 1000 h FCT)
Si – 36 mol% HfO_2	7.64	1.71 (0 – 1000 h FCT)
Si – 60 mol% HfO_2	15.29	9.09 (40 – 800 h FCT)

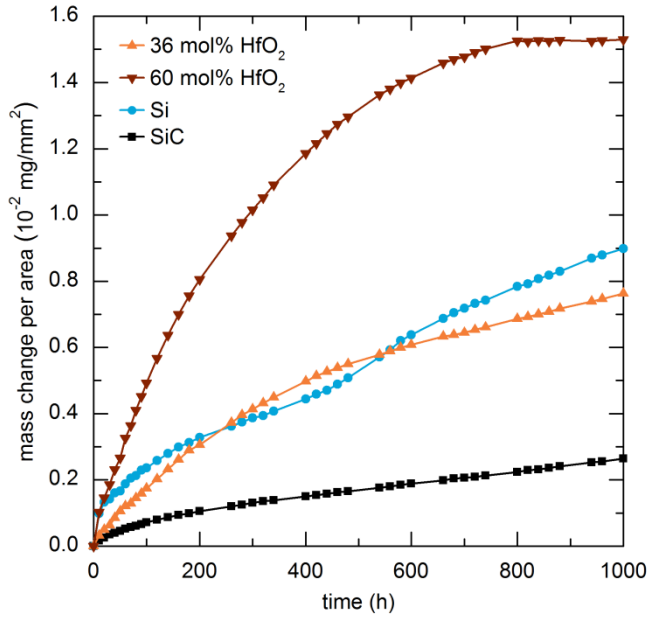

Fig. 13. Mass change per area curves over furnace cycle testing time at 1523 K.

In addition to the mass gain a change in the total thickness of the BCs was found. Fig. 14 illustrates the increase in TGO thickness on the one hand and accordingly the decrease in the remaining non-oxidized layer thickness on the other one. The TGO growth in the left part of Fig. 14 corresponds to the mass change given in Fig. 13 very well. The curves follow the same slopes and the close similarity in oxidation kinetics between the silicon BC and the low hafnia-doped BC becomes visible.

Acta Materialia; Anton et. al. 2020, https://doi.org/10.1016/j.actamat.2019.10.050

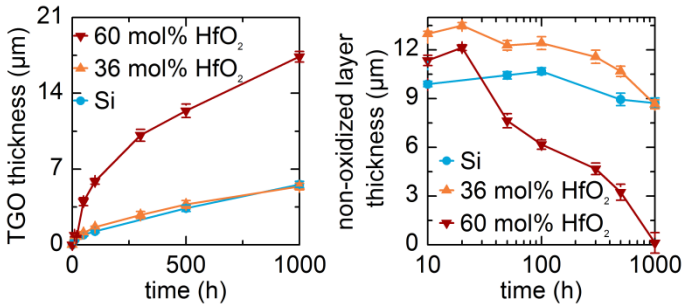

Fig. 14. Left: increase in TGO thickness over the furnace cycle testing time at 1523 K; right: decrease in non-oxidized layer thickness over the FCT time at 1523 K.

EDS line scans and point analyses (not shown here) obtained from cross sections were analysed to further confirm the underlying oxidation progress of the coatings. Once again, it became clear that the lower doped variant has a slowly growing mTGO at a rate comparable to that of the pure silicon BC. The mTGO of the higher doped variant grew much faster instead and lead to complete oxidation of this BC variant after 1000 h.

4.Discussion

4.1.1. Effect of doping content on the microstructure over the course of testing time

The pure silicon BC fabricated by magnetron sputtering behaves similarly to coatings described by other researchers [2,11]. While the deposition parameters or even the deposition process may differ from other publications, this Si-BC also forms a TGO layer due to the exposure to oxygen at high temperatures. Since a columnar structure is typical for a magnetron sputtering process, seen in Fig. 1, the exposed surface of the column boundaries oxidizes first before building up a dense layer on top covering the whole surface of the coating. By continuing the FCT at 1523 K, the TGO thickness increases. Deal calculated the parabolic rate constant of SiO_2 to be about $0.351 \cdot 10^{-4}$ $(mg/cm^2)^2$ 1/min at 1473 K [19] which correlates well with the parabolic rate constant found here for the TGO of the Si-BC of about $0.368 \cdot 10^{-4}$ $(mg/cm^2)^2$ 1/min at 1523 K. The Si-BC oxidation rate appears to be influenced by the internal oxidation occurring along gaps in the columnar structure, see Fig. 13. It is also considerably higher than that of the SiC substrate, the latter one is obviously underestimated since the carbon gets oxidized as well in SiC but it is volatilized which lowers the total mass of the sample. In Fig. 3 A, stress-induced cracks are noticeable in the TGO of the silicon coating. Richards et al. estimated a onset of TGO-channel cracking for a TGO thickness of about 1.5 µm [20]. This is in a good agreement with the findings here. The first appearance of channel cracking was examined after 100 h FCT at a TGO thickness of about 1.3 µm. The reason for crack formation is attributed to the cristobalite phase transition, which has been confirmed by several researchers. The cristobalite phase transition in this work was found to occur at 483 K which is in good agreement with findings in literature [11,21]. At the end of testing, the TGO layer has a critical thickness of about 5.6 µm, which accounts for 39 % of the total thickness (remaining coating plus TGO) after 1000 h FCT. At the interface between un-oxidized silicon and TGO the stresses accumulate and vertical channel cracks convert progressively into mudcracks. This ultimately leads to spallation of the TGO layer in large areas.

Kleebe et al. investigated the coarsening of hafnia in a SiOC matrix. There, hafnia precipitates fall out as spherical shaped particles [22]. The same can be seen here when analysing the hafnia-doped coatings. Starting with the lower doped variant, a homogenous distribution of HfO_2 particles appears after 10 h and

100 h of FCT, see Fig. 2 and Fig. 3 B and C column. Fig. 8 shows rather similar values in feret size for these times throughout the coating. The lower hafnia-doped BC presents a rather slow growing mTGO. After 1000 h FCT, Ostwald ripening can be confirmed in the mTGO, resulting in fewer but larger hafnia particles in the upper part. Thereby, an inhomogeneous distribution of hafnia particles evolves, visible in Fig. 4 in the B column. Fig. 5 provides evidence that the hafnia particle growth in the mTGO is inhomogeneous throughout the coating. Some areas exhibit larger hafnia particles after oxidation for 1000 h while in other areas the particles are still small and relatively homogeneously distributed. EDS analyses suggest that the large particles in the lower doped variant were formed only by reaction of hafnia with silica to hafnon while the smaller particles which are farther from the surface are still mostly hafnia. It is very likely that either local changes of the viscosity of the silica glass or changes in local mobility of oxygen especially along inter-columnar boundaries may have caused those differences.

The reaction between hafnia and silica is more elucidated in Fig. 15. The hafnon formation is confirmed by the XRD findings which reveal the hafnon phase only after 1000 h FCT in the lower doped variant but much earlier in the higher doped BC (Fig. 10). This leads to the conclusion that the mobility of hafnia is enhanced by the formation of silica associated with the reaction among both reactants to hafnon. As hafnon is the thermodynamically favourable phase and the lower doped BC is oxidized only near the surface, there is a driving force for outward diffusion of hafnia to react with silica.

Contrary, with the much faster oxidation of silicon in the higher doped variant which is attributed to the network formation of hafnia, there is no driving force for hafnia diffusing outward. Consequently, in the higher hafnia-doped variant a relative homogeneous particle size distribution within this BC is found. Most of the HfO_2 precipitates are exposed to the same silica matrix phase while in the lower doped variant only the upper part of the matrix consists of silica (mTGO) while the lower part and most likely the areas consisting of smaller Hf-rich particles (see Fig. 5 right picture) is still silicon. Therefore, a more uniform evolution of the precipitates can be observed in the higher doped variant rather than in the lower doped BC with distinct variation in particle size across the coating thickness and along the coating due to different mTGO growth rates. This implies that hafnia coarsens faster in a silica matrix than in silicon, and in addition the reaction to hafnon may further enhance the coarsening rate of particles. Only after 1000 h FCT slightly enlarged particles were detected close to the substrate in the 36 mol% HfO_2 variant (see Fig. 4 B), indicating the slow kinetic of the hafnon transformation.

The relatively sluggish reaction of hafnia with silica at the applied temperature becomes evident in Fig. 7 after 1000 h FCT. Close to the substrate large particles reveal some change in contrast, indicating a core that is still HfO_2 while the rim of the particles has already reacted to hafnon. Since the Hf-containing particles stay dense and transform from the outside inwards, it is evident that mostly SiO_2 diffuses inside those particles. This assumption is supported by findings of Cheraniak who describes the diffusion of zircon or hafnium to be much slower than the diffusion of silicon and oxygen. Because of their similarity in charge and size hafnium and zircon have similar properties [23]. Fig. 15 schematically summarizes the current observations of hafnon formation.

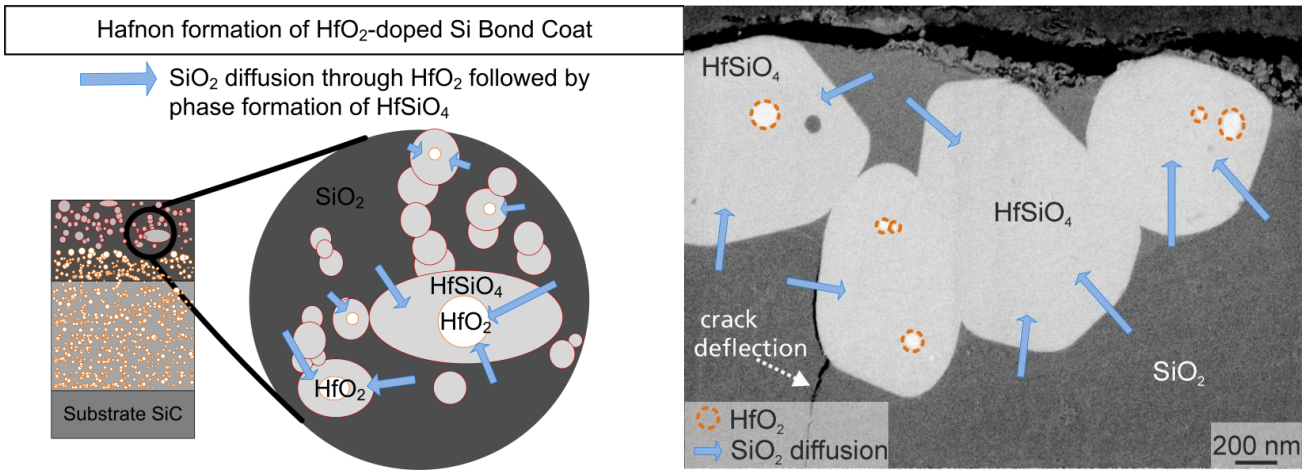

Fig. 15. Schematics of reaction between HfO_2, SiO_2 and $HfSiO_4$ phase formation by mostly diffusion of SiO_2 into HfO_2 (left) and EsB picture of the 36 mol% HfO_2-doped BC (right). The bright particles visible in EsB picture have been circled and evidently they are rich in hafnium.

This mechanism of phase formation is further supported by the TEM analyses for Si and SiO_2. It becomes evident in Fig. 12 B that the core of the SiO_2 region is still rich in Si while the rim is already transformed to cristobalite. Only in areas of silica formation hafnium is present while it is absent in areas of non-oxides silicon. This case is shown in Fig. 16 schematically by the transformation in the mTGO.

4.1.2. Effect of doping content on the phase formation over the course of testing time

After deposition the BCs are X-ray amorphous which is the usual state of many sputtered coatings [2,24]. The BCs are fully crystallized after the first heat treatment. Silicon and cristobalite are detected in all variants. Since the cristobalite high/low temperature phase transition has been proven by high temperature XRD it can be assumed that locally large CTE mismatches between the phases appear at lower temperatures. Alpha cristobalite with a CTE of $10.3 \cdot 10^{-6}$ K^{-1} is rather unsuitable in comparison to the beta high temperature phase with a CTE of $3.1 \cdot 10^{-6}$ K^{-1}. A second deleterious effect originates from the volume change of about 4.3 % caused by this polymorphic transition. In the pure silicon BC, the mismatch elicits tension and cracks. Previous studies proved the cristobalite phase transition to be the dominating factor for tension and mud cracking in the TGO [11,21]. Therefore, the same holds here for the pure silicon BC and its cracking and spalling TGO. A different reaction is shown by the doped coatings which seem to be able to balance the CTE mismatch much better. They do not severely crack in the early phases of cyclic oxidation. The transformation of HfO_2 and SiO_2 into $HfSiO_4$ at around 300 h or 1000 h FCT, depending on the doping content, is most likely the reason for the resistance of the coatings against tension induced cracking. The volume expansion due to the hafnon formation can explain the lower tendency of hafnia-doped silicon BCs to cracking. Y. Shinoda et al. describe a volume increase from SiC and HfO_2 of 13.8 % when turning into $HfSiO_4$. In the present case of silicon that oxidizes to silica and reacts with hafnia forming hafnon in the BC the volume increase has been calculated to be 14.8 % [18]. The TEM/EDS mapping confirms that the hafnon transformation first starts within the SiO_2. In Fig. 12 A no distinguished separation of silicon can be seen, whereas in Fig. 12 B silicon is clearly not mixed with the hafnia-rich phases. This supports the XRD scans where both HfO_2 and $HfSiO_4$ can be found in the 60 mol% doped variant after 500 h testing and in the 36 mol% doped one after 1000 h testing. $HfSiO_4$ has a lower CTE than HfO_2 and can potentially decrease the cristobalite/silicon CTE mismatch. This can be seen in Table 2 where the CTEs of the coatings are calculated based on the measured phase contents for the testing time of 10, 100 and 1000 h in the high and low temperature state.

The CTE values were taken from literature [10,11,18,25,26] and phase percentages given by Rietveld analyses made an approximate evaluation of the overall BC CTE possible. Even though, the overall CTE at room temperature is slightly higher than the CTE of SiC and of pure silicon, the CTE at 1523 K continuous to be stable throughout the testing. This is a major indication why the doped coatings did not show spallation of the oxide.

Table 2 Calculated CTE for all BC variations at room temperature and 1523 K. The pure Si bond coat has a value of $2.6 \cdot 10^{-6}$ K^{-1} at 298 K and $4.6 \cdot 10^{-6}$ K^{-1} at 1500 K [10].

		CTE in variation (10^{-6} K^{-1})	
Time (h)	Temperature (K)	60 mol% HfO_2	36 mol% HfO_2
10	298	4.56	3.39
	1523	4.61	4.53
100	298	5.60	5.10
	1523	4.41	4.27
1000	298	7.13	5.86
	1523	4.47	4.20

4.1.3. Effect of doping content on the oxidation behaviour over the course of testing time

Since one main task of a bond coat is to protect the substrate against oxidation, the development of a dense, well adherent, and homogeneous TGO layer is wanted. Problems will occur when the oxide layer becomes too thick and/or the CTE mismatch is too high which causes tension within the coating. Eventually, they will induce cracks and the thermomechanical stresses during transient heating and rapid cooling leads to spallation. Therefore, aiming for a slowly growing oxide scale and for a low CTE mismatch is one of the main concerns for the bond coat within an EBC system.

All variants show passive oxidation behaviour over the course of the testing. This can be seen in Fig. 13 by the shape of the curves. Thus, the oxidation mechanisms of all coatings follow parabolic oxidation kinetics. Several researchers have already shown passive oxidation for silica which is in excellent agreement to the results shown here [2,27]. The low hafnia content BC develops a mTGO consisting of silica and hafnia in the earlier stages of oxidation and a mixture of silica, hafnia and hafnon in the later stage. Here, the hafnia/hafnon particles seem to have almost no influence on the growth rate of the mTGO. Since the serial sectioning analysis did not reveal a continuous network of hafnia particles in the lower doped BC, it can be assumed that hafnia has only a limited influence on the oxygen diffusion in this variant and hence on the oxidation process. Table 1 shows an even lesser k_p value for the lower doped BC than the Si-BC. The oxidation rate can be considered the same since analytical errors have to be considered. The high hafnia content BC has a fast growing mTGO where the oxygen travels fast through the continuous hafnia network. This is in good agreement with Goncharova et al. who found the activation barrier for SiO_2 growth at a HfO_2/Si and $HfSiO_x$/Si interfaces much lower than that at the SiO_2/Si interface. The reason seems to be in the predominant diffusion mechanism in hafnia involving the continuous replacement of an oxygen lattice site by the diffusion defect [28]. Furthermore, grain or phase boundary diffusion at the Si/HfO_2 interface cannot be excluded to presumably contribute to the accelerated oxygen diffusion. To summarize the findings and to support this argument a schematic drawing is given in Fig. 16 describing the oxygen diffusion in the current high doped BC that is characterized by a nearly continuous network of connected hafnia particles. Although the oxide layer thickness and the oxidation rate have increased in comparison to the pure Si-BC and the 36 mol% HfO_2 BCs, the coating shows a good adhesion and just few cracks without spallation.

Acta Materialia; Anton et. al. 2020, https://doi.org/10.1016/j.actamat.2019.10.050

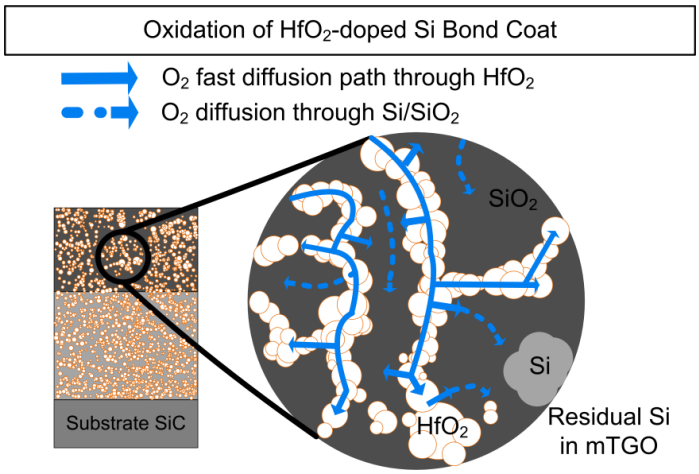

Fig. 16. Schematic of the oxidation of the high hafnia-doped coatings by fast diffusion paths through or along connected hafnia particles and slower diffusion through Si/SiO_2.

In order to conclude the findings, changes in phase assemblage, particle size and distribution, oxide growth, and microstructure over testing time are schematically shown in Fig. 17.

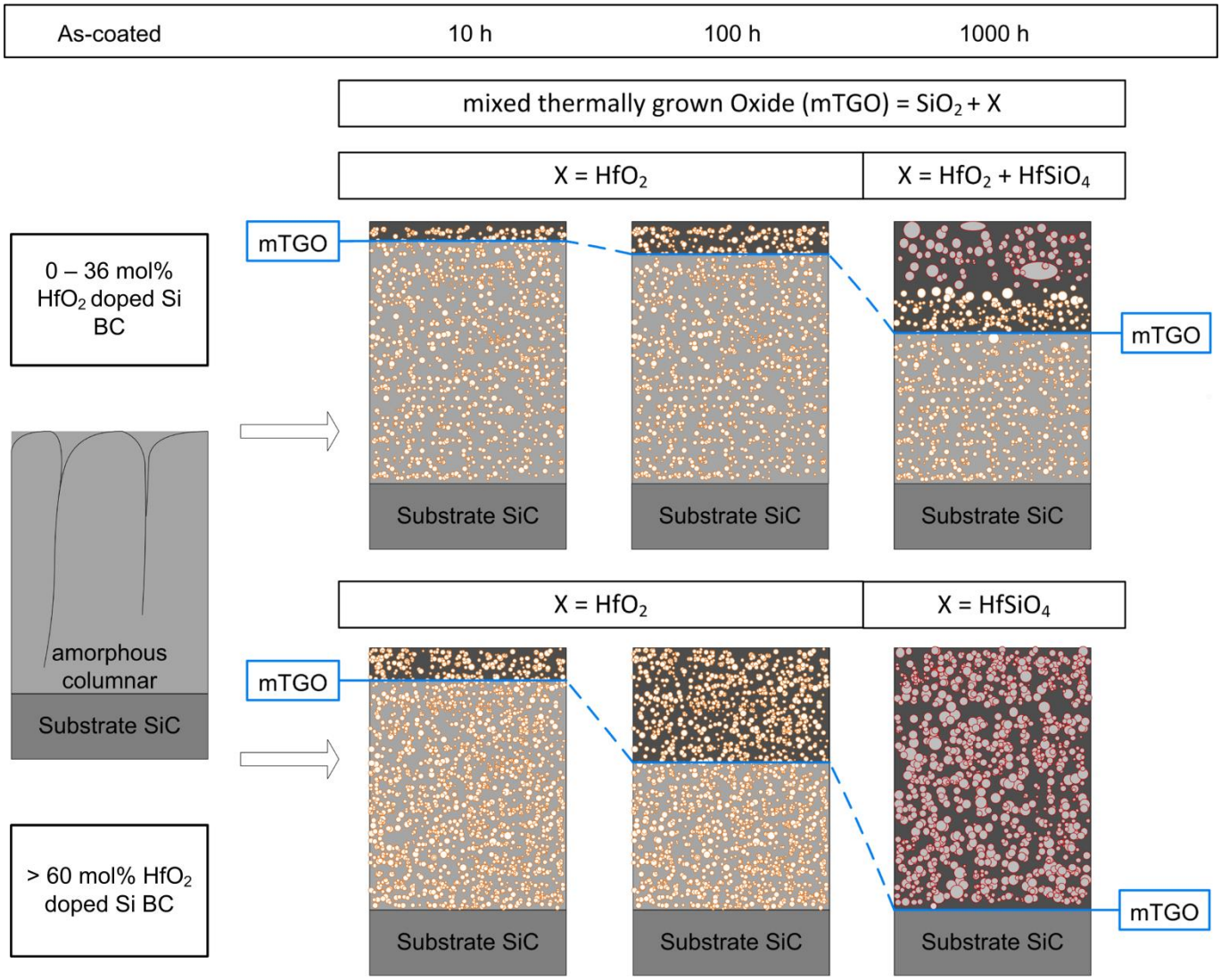

Fig. 17. Schematic evolution of hafnia-doped Si-BCs during various FCT stages showing the increase of the mTGO and the phase formation. The blue line symbolises the interface between mTGO and the remaining BC.

Acta Materialia; Anton et. al. 2020, https://doi.org/10.1016/j.actamat.2019.10.050

The hafnia-doped Si-BCs react under thermal cycling testing conditions at 1523 K in the following manner. The lower doped variant oxidizes more slowly and shows after 1000 h a two-layer structure comprising an upper oxidized part of silica, hafnia and hafnon as a reaction product from silica and hafnia and a lower un-oxidized part. There can be still a small portion of initial silicon in the mTGO. The initial BC underneath has residual silicon plus hafnia. Substantial coarsening of the hafnon particles in the upper layer is evident, indicating a higher coarsening rate of either hafnia within silica or of hafnon within silica, or possibly of both. The higher doped variant forms a network of connected hafnia particles, giving rise to fast inward diffusion of oxygen. Consequently, the oxidation is much faster and finally a relatively homogenous layer of completely oxidized silica plus hafnon forms. XRD shows that after 1000 h the silicon transformed into SiO_2 and the hafnia has fully reacted with silica to hafnon.

5. Conclusions

The results prove the feasibility and advantages of magnetron sputtered refractory metal oxide doped Si bond coats deposited on SiC substrates, intended as the first layer within an EBC system for SiC/SiC CMCs. Hafnia had been used as dopant in two different amounts, namely 36 mol% and 60 mol%, and was compared to a pure silicon BC.

All coatings were X-ray amorphous and dense with a columnar structure after deposition. During furnace cycle testing at 1523 K for up to 1000 h the bond coats crystallized rapidly and hafnia fell out as spherical precipitates. All variants showed an increasing (mixed) thermally grown oxide thickness with time that consists at the beginning mainly of SiO_2 and SiO_2/HfO_2. The oxidation heavily depended on the dopant content in the bond coat. During testing, Ostwald ripening increased the size of the precipitates. The high temperatures and long testing times also favoured a sluggish phase formation of hafnon in the mTGO out of hafnia and SiO_2.

3D image analyses have proven that in the 60 mol% HfO_2 BC a network of hafnia particles within the BC has formed, leading to fast diffusion of oxygen into the coating and therefore to an increased oxidation rate. In the 36 mol% coating, no continuous network formation like in the 60 mol% hafnia BC could be observed. Therefore, the lower doped BC had the same oxidation rate than a pure Si-BC since the isolated hafnia particles seem not to largely affect the oxidation.

While the thermally grown oxide on the pure silicon BC showed severe mud cracking and oxide spallation after 1000 h FCT, both doped variants showed an excellent oxide adhesion and no spallation was observed, despite of remarkable differences in oxidation rates. Within the SiO_2 phase hafnia transformed into hafnon at different rates depending on the hafnia content. The hafnon formation is assumed to compensate the CTE mismatches occurring from the cristobalite high/low temperature phase change which seems to suppress crack formation in the bond coat.

All three bond coats provide protection of the underlying SiC up to 1000 h cyclic testing with a more favourable behaviour of the HfO_2-doped bond coats. Further tests especially of a full EBC system under water vapour resistance will follow in the near future to verify the functionality of the novel bond coats to improve EBC performance as a whole.

6. Acknowledgment

For the technical support at the DLR – German Aerospace Center the authors thanks A. Handwerk.

7. References

[1] R.C. Robinson, J.L. Smialek, SiC Recession Caused by SiO 2 Scale Volatility under Combustion Conditions : I , Experimental Results and Empirical Model, Ceramics. 25 (1999) 1817–1825. doi:10.1111/j.1151-2916.1999.tb02004.x.

[2] V. Leisner, A. Lange, P. Mechnich, U. Schulz, Magnetron sputtered Y2SiO5 environmental barrier coatings for SiC/SiC CMCs, Ceram. Trans. 263 (2018) 197–209. doi:10.1002/9781119407270.ch20.

[3] H.E. Eaton, G.D. Linsey, Accelerated oxidation of SiC CMC's by water vapor and protection via environmental barrier coating approach, J. Eur. Ceram. Soc. 22 (2002) 2741–2747. doi:10.1016/S0955-2219(02)00141-3.

[4] R.A. Golden, E.J. Opila, A method for assessing the volatility of oxides in high-temperature high-velocity water vapor, J. Eur. Ceram. Soc. 36 (2016) 1135–1147. doi:10.1016/j.jeurceramsoc.2015.11.016.

[5] N.L. Ahlborg, D. Zhu, Calcium-magnesium aluminosilicate (CMAS) reactions and degradation mechanisms of advanced environmental barrier coatings, Surf. Coatings Technol. 237 (2013) 79–87. doi:10.1016/j.surfcoat.2013.08.036.

[6] D.L. Poerschke, D.D. Hass, S. Eustis, G.G.E. Seward, J.S. Van Sluytman, C.G. Levi, Stability and CMAS resistance of ytterbium-silicate/hafnate EBCs/TBC for SiC composites, J. Am. Ceram. Soc. 98 (2015) 278–286. doi:10.1111/jace.13262.

[7] K.M. Grant, S. Krämer, J.P.A. Löfvander, C.G. Levi, CMAS degradation of environmental barrier coatings, Surf. Coatings Technol. (2007). doi:10.1016/j.surfcoat.2007.06.045.

[8] B.T. Richards, H.N.G. Wadley, Plasma spray deposition of tri-layer environmental barrier coatings, J. Eur. Ceram. Soc. 34 (2014) 3069–3083. doi:10.1016/j.jeurceramsoc.2014.04.027.

[9] K.N. Lee, Environmental Barrier Coatings for SiCf/SiC, in: Ceram. Matrix Compos. Mater. Model. Technol., 2014: pp. 430–451. doi:10.1002/9781118832998.ch15.

[10] Y. Okada, Y. Tokumaru, Precise determination of lattice parameter and thermal expansion coefficient of silicon between 300 and 1500 K, J. Appl. Phys. (1984). doi:10.1063/1.333965.

[11] B.T. Richards, S. Sehr, F. De Franqueville, M.R. Begley, H.N.G. Wadley, Fracture mechanisms of ytterbium monosilicate environmental barrier coatings during cyclic thermal exposure, Acta Mater. 103 (2016) 448–460. doi:10.1016/j.actamat.2015.10.019.

[12] H. Salmang, H. Scholze, R. Telle, Keramik, 2007. http://link.springer.com/content/pdf/10.1007/978-3-540-49469-0.pdf.

[13] W.D. Sylwestrowicz, Mechanical properties of single crystals of silicon, Philos. Mag. 7 (1962) 1825–1845. doi:10.1080/14786436208213849.

[14] D. Zhu, Development and Performance Evaluations of HfO 2 -Si and Rare Earth-Si Based Environmental Barrier Bond Coat Systems for SiC / SiC Ceramic Matrix Composites NASA EBC and CMC System Development, 41st Int. Conf. Metall. Coatings Thin Film. (2014).

[15] K.N. Lee, Protective coatings for gas turbines, Gas Turbine Handb. 4 (2006) 419–437.

[16] T. Ohji, M. Singh, Engineered Ceramics, John Wiley & Sons, Inc., Hoboken, NJ, USA, 2016. doi:10.1002/9781119100430.

[17] A.L. Robertson, F. Solá, D. Zhu, J. Salem, K.W. White, Microscale fracture mechanisms of HfO2-Si environmental barrier coatings, J. Eur. Ceram. Soc. (2019). doi:10.1016/j.jeurceramsoc.2019.02.001.

[18] Y. Shinoda, D.B. Marshall, R. Raj, Oxidation, mechanical and thermal properties of hafnia-silicon carbide nanocomposites, J. Eur. Ceram. Soc. 34 (2014) 1783–1790. doi:10.1016/j.jeurceramsoc.2013.12.044.

[19] B.E. Deal, The Oxidation of Silicon in Dry Oxygen, Wet Oxygen, and Steam, J. Electrochem. Soc. 110 (2007) 527. doi:10.1149/1.2425807.

[20] B.T. Richards, K.A. Young, F. De Francqueville, S. Sehr, M.R. Begley, H.N.G. Wadley, Response of ytterbium disilicate-silicon environmental barrier coatings to thermal cycling in water vapor, Acta Mater. 106 (2016) 1–14. doi:10.1016/j.actamat.2015.12.053.

[21] Y. Arai, Y. Aoki, Y. Kagawa, Effect of cristobalite formation on the delamination resistance of an oxide/Si/(SiC/SiC) environmental barrier coating system after cyclic high temperature thermal exposure, Scr. Mater. 139 (2017) 58–62. doi:10.1016/j.scriptamat.2017.06.006.

[22] H.J. Kleebe, K. Nonnenmacher, E. Ionescu, R. Riedel, Decomposition-coarsening model of SiOC/HfO 2ceramic nanocomposites upon isothermal anneal at 1300°C, J. Am. Ceram. Soc. 95 (2012) 2290–2297. doi:10.1111/j.1551-2916.2012.05227.x.

[23] D.J. Cherniak, Si diffusion in zircon, Phys. Chem. Miner. 35 (2008) 179–187. doi:10.1007/s00269-007-0210-6.

[24] P. Mechnich, A. Lange, R. Braun, C. Büttner, Y2SiO5 coatings fabricated by RF magnetron sputtering, Surf. Coatings Technol. 237 (2013) 88–94. doi:10.1016/j.surfcoat.2013.08.015.

[25] É. Darthout, F. Gitzhofer, Thermal Cycling and High-Temperature Corrosion Tests of Rare Earth Silicate Environmental Barrier Coatings, J. Therm. Spray Technol. 26 (2017) 1823–1837. doi:10.1007/s11666-017-0635-5.

[26] S. Ueno, D.D. Jayaseelan, H. Kita, T. Ohji, H.T. Lin, Comparison of Water Vapor Corrosion Behaviors of $Ln_2Si_2O_7$ (Ln=Yb and Lu) and $ASiO_4$ (A=Ti, Zr and Hf) EBC's, Key Eng. Mater. 317–318 (2006) 557–560. doi:10.4028/www.scientific.net/KEM.317-318.557.

[27] H.E. Eaton, G.D. Linsey, Accelerated oxidation of SiC CMC's by water vapor and protection via environmental barrier coating approach, J. Eur. Ceram. Soc. 22 (2002) 2741–2747. doi:10.1016/S0955-2219(02)00141-3.

[28] L. V. Goncharova, M. Dalponte, T. Feng, T. Gustafsson, E. Garfunkel, P.S. Lysaght, G. Bersuker, Diffusion and interface growth in hafnium oxide and silicate ultrathin films on Si(001), Phys. Rev. B - Condens. Matter Mater. Phys. 83 (2011). doi:10.1103/PhysRevB.83.115329.